Nonlinear cooling of an annular beam distribution

A. Bazzani,[1] F. Capoani,[1,2] M. Giovannozzi,[2,*] and R. Tomás[2]

[1]*Dipartimento di Fisica e Astronomia, Università di Bologna and INFN Bologna, via Irnerio 46, Bologna, Italy*

[2]*Beams Department, CERN, Esplanade des Particules 1, 1211 Geneva 23, Switzerland*

(Received 6 May 2022; accepted 17 January 2023; published 2 February 2023)

In recent years, intense efforts have been devoted to studying how nonlinear effects can be used to shape the transverse beam distribution by means of an adiabatic crossing of nonlinear resonances. By this approach, it is possible to split the beams in the transverse plane so that the initial single-Gaussian beam is divided into several distinct distributions. This is at the heart of the multiturn extraction process that is successfully in operation at the CERN Proton Synchrotron. Nonlinear effects can also be used to cool a beam by acting on its transverse beam distribution. In this paper, we present and discuss the special case of a beam with an annular distribution, showing how its emittance can be effectively reduced by means of properly devised manipulations based on nonlinear effects.

DOI: 10.1103/PhysRevAccelBeams.26.024001

I. INTRODUCTION

Nonlinear effects introduce new beam dynamics phenomena that might open up the possibility of devising novel beam manipulation techniques. This is the case, for instance, when shaping the transverse beam distribution by means of the adiabatic crossing of a stable nonlinear resonance. This process is at the heart of the so-called beam splitting that is used for CERN Multiturn Extraction (MTE) [1–3] and has been successfully implemented as a routine part of the CERN Proton Synchrotron operation for several years [4–6].

However, this is not the only nonlinear manipulation that can be devised. Indeed, under the inspiration of [7], it has been found that a controlled redistribution of the invariants can be achieved between the two transverse degrees of freedom [8], provided that an appropriate two-dimensional nonlinear resonance is crossed. This opens novel options in terms of manipulation of the transverse beam emittances.

It is, therefore, natural to study whether nonlinear effects can be used efficiently to reduce the linear invariants of a transverse beam distribution, thus generating a cooling of the transverse beam emittance. The basis of this approach to beam cooling is the observation that nonlinear effects do not preserve the linear invariant, i.e., the linear action, or the so-called Courant-Snyder invariant. In this sense, they can be used to reduce the value of the linear invariant without violating the symplectic character of the Hamiltonian dynamics. Therefore, comparing the value of the linear invariant before and after the action of nonlinear forces, i.e., when the dynamics is linear and expressed as a rotation around the origin of the phase space, is a correct indicator of the reduction of the invariant for each individual particle, hence of the entire beam distribution and of the corresponding emittance.

In this paper, the initial step toward the development of a nonlinear cooling of a particle distribution is discussed. We present a framework to cool an annular beam distribution, i.e., a distribution with nonzero density in an interval of radii $r_1 < r < r_2, r_1 > 0$ in the normalized phase space. It is well known that annular beam distributions are generated as the result of applying a single transverse kick to a centered beam in the presence of decoherence. Hence, a potential application of annular beam cooling could be the restoration of the initial centered distribution after a transverse kick.

It is worth recalling the two well-established techniques, namely electron cooling [9] and stochastic cooling [10], which represent the options available to manipulate the transverse emittances of a charged particle beam. The first relies on creating an equilibrium between the circulating beam and an electron beam that provides cooling to the circulating particles. The latter reduces the beam emittances by imparting a dipole kick of appropriate amplitude, determined upon a beam measurement performed by a dedicated beam position monitor. These two cooling techniques are clearly very different with respect to the proposed cooling based on nonlinear effects. First, in terms of the physical phenomenon used to achieve cooling; second, in terms of the hardware needed to implement

*Corresponding author.
massimo.giovannozzi@cern.ch

the various approaches, as the well-established cooling principles rely on complicated hardware devices, which is not the case for the proposed cooling mechanism. Last, the domain of applicability contrasts the three methods: electron and stochastic cooling being very general, the newly proposed one being very specific, as it applies only to a certain beam distribution. Worth mentioning is also laser cooling, another cooling technique that, however, is applicable only to certain ion species and over a limited range of beam energy values (see, e.g., [11–19] for a selection of references on this topic).

A general discussion of the systems that can be used to devise a cooling method for an annular beam distribution is presented in Sec. II, while the considered models are presented in Sec. III together with some results of the adiabatic trapping theory applied to the models. In the same section, several cooling protocols are defined, and their performance is analyzed in detail using extensive numerical simulations, the results of which are presented and discussed in Sec. IV. Finally, conclusions are drawn in Sec. V, with some mathematical details reported in the appendix.

II. CONSIDERATIONS ON THE MODEL CHOSEN

A. General aspects

The general idea underlying the approach developed to achieve cooling of the emittance of an annular beam distribution is based on creating stable islands in phase space. This can be done by slowly varying the parameters to vary the area of the islands to cause the particles to cross the separatrices. When the resonance islands are moved in phase space, the action can be changed and eventually reduced.

To create stable phase-space islands, a resonance needs to be excited. The MTE experience suggests using a Hénonlike map as a model, close to stable low-order resonances, e.g., $1/4$, $1/5$. If the initial annulus lies outside the chain of islands, then by changing the linear frequency, one can act on the area of the central region and of the islands to trap particles in the center. This reduces the action by a quantity equivalent to the area of the islands divided by 2π, according to the separatrix crossing theory.

A simple analysis of the scaling laws of the parameters of the islands, found in [20], suggests that this approach is feasible only for resonances of order $n = 4$. However, to obtain the best cooling results, two parameters are needed to control the position and area of the resonance islands. Using the sextupole coefficient is not efficient, since it acts as a global scale parameter [20] and therefore changes the dynamic aperture of the map. Therefore, an octupole kick should be added to the sextupole one to provide an additional free parameter. Estimates for the island area and the central region can be derived using the results of [20] and [21]. However, the main drawback of this approach is the thick stochastic layer generated by the octupole kick around the outer part of the separatrix of the four stable islands. This has the effect of inducing particle loss, making the method unreliable. These observations make the approach based on Hénon-like maps unsuitable for the application under consideration.

Ongoing studies indicate that trapping in islands and transport from within islands can also be achieved efficiently using ac-modulated magnets [22]. The most straightforward option consists of creating an island using an ac dipole in a $1:1$ resonance condition, i.e., with the oscillation frequency close to the linear tune of the system. It is worth recalling that ac dipoles have been widely studied in the field of accelerator physics, with essential applications to beam diagnostics (see, e.g., [23–30], for an overview of ac dipole studies and applications). Therefore, a cooling method for annular beams will be devised based on the Hamiltonian system modeling of the stable islands used to perform the adiabatic trapping and subsequent transport under the influence of an ac dipole.

B. Phase-space dimension

The fundamental idea behind the proposed application of nonlinear dynamics to reduce the emittance of an annular beam consists of using magnets that generate nonlinear fields, e.g., sextupoles, and an ac dipole that generates an oscillatory field. It is not restrictive to assume that the annular distribution occurs in the horizontal phase space. Therefore, the ac dipole will also act in this plane. However, the sextupoles act on both horizontal and vertical planes, introducing a nonlinear coupling between the two transverse degrees of freedom. Therefore, based on these simple considerations, the model that describes the cooling process should be defined in a 4D phase space. However, the dimensionality of the model can be reduced to two dimensions only, provided that the sextupoles are located in sections of the ring where the horizontal beta function (β_x) is larger than the vertical one (β_y), which seems to be a rather mild constraint. Another possibility, though inducing a stronger constraint, is to use a beam in which the vertical emittance is smaller than that of the annular distribution in the horizontal plane. These qualitative considerations have been quantitatively confirmed in the framework of studies (experimental, theoretical, and numerical) carried out to implement the CERN MTE. This beam manipulation is carried out in the horizontal plane and is performed using sextupoles and octupoles that have been installed in straight sections in which $\beta_x \approx 2\beta_y$ [31] and the impact on the vertical emittance due to the cross of the horizontal resonance is very small [6]. More precisely, over the intensity range of 1.5–2×10^{13} protons per pulse, the vertical emittance [32] features a growth in the range of 10%–16%. This growth is computed from injection to just before extraction, and the sextupoles and octupoles act only shortly before extraction. Therefore, the reported emittance growth clearly also includes the effects of all possible

sources of emittance increase, unrelated to the nonlinear magnets inducing beam splitting. This indicates that the nonlinear coupling caused by MTE is only a fraction of the measured emittance growth and that the strategy to mitigate the nonlinear coupling is fully successful.

These arguments can be mathematically rigorous. The system under consideration is described by the following Hamiltonian:

$$\mathcal{H}(x,p_x,y,p_y,t)=\omega_{0,x}\frac{x^2+p_x^2}{2}+\omega_{0,y}\frac{y^2+p_y^2}{2}+\frac{k_3}{3}(x^3-3xy^2)+\varepsilon x\cos\omega t, \quad (1)$$

where the coordinates used are the Courant-Snyder coordinates [33]. This Hamiltonian can be studied using perturbative techniques, such as normal forms (see, e.g., [34]). In the case that the linear tunes $\omega_{0,x},\omega_{0,y}$ are not close to a low order resonance condition, the unperturbed Hamiltonian (1) ($\varepsilon=0$) is quasi-integrable in a neighborhood of the origin and one can introduce action angle variables (ϕ_x,J_x) and (ϕ_y,J_y). Moreover, since we are interested in the linear resonance $\omega_{0,x}-\omega=0$, it is sufficient to consider the leading term in the time-dependent perturbation theory, applying an averaging procedure for the other Fourier components [35]. Therefore, in the action angle variables, it is possible to reduce the Hamiltonian (1) to the form

$$\mathcal{H}(\phi_x,J_x,\phi_y,J_y,t)=\omega_{0,x}J_x+\omega_{0,y}J_y+\frac{\Omega_{xx}}{2}J_x^2+\frac{\Omega_{yy}}{2}J_y^2+\Omega_{xy}J_xJ_y+\varepsilon\sqrt{2J_x}\cos\phi_x\cos\omega t. \quad (2)$$

We observe that $\mathcal{H}$ does not depend on ϕ_y, which implies that J_y is an invariant. Therefore, system (1) can be described by the following Hamiltonian:

$$\mathcal{H}(\phi_x,J_x,t)=\omega_{0,x}J_x+\frac{\Omega_{xx}}{2}J_x^2+\Omega_{xy}J_xJ_y+\varepsilon\sqrt{2J_x}\cos\phi_x\cos\omega t, \quad (3)$$

in which J_y is a parameter. Furthermore, the system can be designed so that $\Omega_{xy}\ll 1$, which reduces the dynamics to a one-dimensional pure case.

III. THEORY

A. The Hamiltonian model

Horizontal betatron motion in the presence of an ac dipole can be described by the Hamiltonian of a generic oscillator with sextupole nonlinearity and dipolar time-dependent excitation [23–25], namely,

$$\mathcal{H}(x,p_x,t)=\omega_0\frac{x^2+p_x^2}{2}+\frac{k_3}{3}x^3+\varepsilon x\cos\omega t, \quad (4)$$

where x and p_x are Courant-Snyder coordinates [33], and

$$k_3=\frac{1}{B_0\rho}\frac{\partial^2 B_y}{\partial x^2}\ell, \quad (5)$$

where $B_0\rho$ stands for the magnetic rigidity of the reference particle, B_y is the transverse component of the magnetic field, and ℓ is the physical length of the magnetic element. We remark that the choice of the sextupole nonlinearity is rather arbitrary, as other types of nonlinearity might be used, as long as they generate an amplitude-detuning term. On the other hand, from the standpoint of applications, the use of a sextupole nonlinearity is very convenient, as it is present in all magnetic lattices of circular accelerators.

Using the normal form approach to determine the nonresonant interpolating Hamiltonian of (4) (see, e.g., [20]) and expressing it in the action angle coordinates (ϕ,J) of the unperturbed ($\varepsilon=0$) system, the Hamiltonian reads as

$$\mathcal{H}(\phi,J,t)=\omega_0 J+\frac{\Omega_2}{2}J^2+\varepsilon\sqrt{2J}\cos\phi\cos\omega t, \quad (6)$$

where $\Omega_2=g(\omega_0)k_3^2$ and $g(\omega_0)$ is a function of the linear frequency [20] given by

$$g(\omega_0)=-\frac{5}{6\omega_0}, \quad (7)$$

which is obtained applying the Poincaré-Von Zeipel perturbation theory to Eq. (4). The quantity Ω_2 represents an amplitude detuning term. We recall that $J(x,p_x)$ is an adiabatic invariant of the unperturbed system if the frequency ω_0 slowly changes.

If we change the coordinates to refer the system to a rotating reference frame with slow angle $\gamma=\phi-\omega t$, taking into account the generating function $F=J(\phi-\omega t)$ and its time derivative $\partial F/\partial t=-\omega J$, the transformation gives

$$\mathcal{H}(\gamma,J,\psi)=(\omega_0-\omega)J+\frac{\Omega_2}{2}J^2+\varepsilon\sqrt{2J}\cos(\gamma+\psi)\cos\psi, \quad (8)$$

where $\psi=\omega t$.

One can average the fast variable ψ using

$$\frac{1}{2\pi}\int_0^{2\pi}\mathrm{d}\psi\,\cos(\gamma+\psi)\cos\psi=\frac{1}{2}\cos\gamma, \quad (9)$$

yielding the new averaged Hamiltonian,

$$\mathcal{H}(\gamma, J) = (\omega_0 - \omega)J + \frac{\Omega_2}{2}J^2 + \frac{\varepsilon}{2}\sqrt{2J}\cos\gamma, \tag{10}$$

which, after a rescaling, can be written in the following form:

$$\mathcal{H}(\gamma, J) = 4J^2 - 2\lambda J + \mu\sqrt{2J}\cos\gamma, \tag{11}$$

where

$$\lambda = \frac{4}{\Omega_2}(\omega - \omega_0), \qquad \mu = \frac{4\varepsilon}{\Omega_2}. \tag{12}$$

Equation (11) represents a well-known Hamiltonian [35,36] that can be conveniently written in the form

$$\mathcal{H}(X, Y) = (X^2 + Y^2)^2 - \lambda(X^2 + Y^2) + \mu X \tag{13}$$

using the Cartesian coordinates $X = \sqrt{2J}\cos\gamma$, $Y = \sqrt{2J}\sin\gamma$. When $\lambda > (3/2)\mu^{2/3}$, a hyperbolic fixed point exists only for $Y = 0$ and

$$X = x_c = \frac{\sqrt{6\lambda}}{3}\cos\left(\frac{\pi}{6} + \alpha\right), \tag{14}$$

where

$$\alpha = \frac{1}{3}\operatorname{asin}\left(\frac{3\sqrt{6}}{4}\frac{\mu}{\lambda^{3/2}}\right). \tag{15}$$

The phase-space portrait of the Hamiltonian (13) is shown in Fig. 1, and it can be divided into three regions:

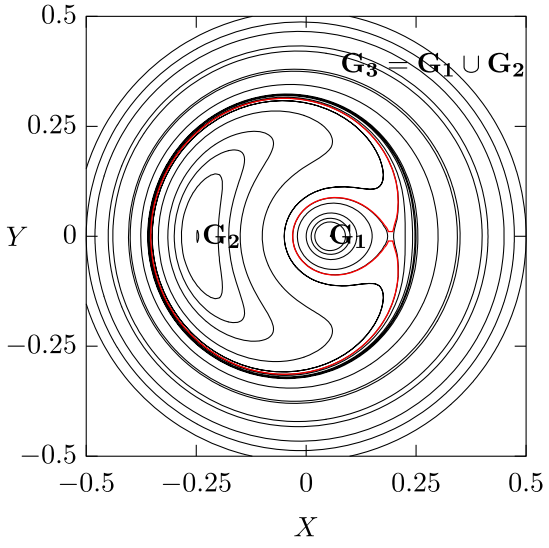

FIG. 1. Phase-space portrait of the Hamiltonian (13) with parameters $\lambda = 0.1$, $\mu = 0.01$. The red line represents the separatrix.

the inner regions G_1 and G_2 (and $G_3 = G_1 \cup G_2$) and the region outside them.

Let us compute the area A_i of any region G_i. If $\mathcal{H}_c$ is the value of the Hamiltonian in $(X = x_c, Y = 0)$, the equation $\mathcal{H}(\gamma, J) = \mathcal{H}_c$ has the solution

$$J(\gamma) = \frac{\lambda - 2x_c^2}{2} - 2x_c\sqrt{\lambda - 2x_c^2}\sin\gamma + 2x_c^2\sin^2\gamma, \tag{16}$$

and $J(\gamma) = 0$ for $\gamma = \gamma_0$ with

$$\gamma_0 = \operatorname{asin}\frac{\sqrt{\lambda - 2x_c^2}}{2x_c}. \tag{17}$$

The area of G_1 in polar coordinates is thus given by

$$A_1 = \int_{-\gamma_0}^{\pi-\gamma_0} d\gamma\, J(\gamma) = \frac{\pi\lambda}{2} - K_1 - K_2, \tag{18}$$

while the area of G_3 is given by

$$A_3 = \int_{-\pi-\gamma_0}^{\gamma_0} d\gamma\, J(\gamma) = \frac{\pi\lambda}{2} + K_1 + K_2 \tag{19}$$

so that

$$A_2 = A_3 - A_1 = 2(K_1 + K_2), \tag{20}$$

where

$$K_1 = \lambda\operatorname{asin}\left(\frac{\sqrt{\lambda - 2x_c^2}}{2x_c}\right), \tag{21}$$

$$K_2 = \frac{3}{2}\sqrt{\lambda - 2x_c^2}\sqrt{6x_c^2 - \lambda}. \tag{22}$$

Let us now consider a particle that lies in the outer region with an action $J_0 > A_3/(2\pi)$. The area enclosed by its orbit will be $A_0 = 2\pi J_0$. If we start a slow change in parameters $\lambda = \lambda(t)$, $\mu = \mu(t)$, according to the theory of adiabatic separatrix crossing [36,37], at $t = t^*$, when the condition $A_3 = A_0$ is met for $\lambda = \lambda^*$, $\mu = \mu^*$, the particle is captured in G_1 or G_2 as a random event. Defining

$$\xi_i = \frac{dA_i/dt}{dA_3/dt} \qquad i = 1, 2, \tag{23}$$

the probability P_i of trapping in G_i, $i = 1, 2$ is given by

$$P_i = \begin{cases} 1 & \text{if } \xi_i > 1 \\ \xi_i & \text{if } 0 < \xi_i < 1 \\ 0 & \text{if } \xi_i < 0 \end{cases}. \tag{24}$$

After trapping, the resulting action J is given by $A_i/(2\pi)$, where A_i is calculated when trapping occurs, that is, for $\lambda = \lambda^*$ and $\mu = \mu^*$.

Given an initial distribution of particles, all of which have an initial action in the neighborhood of J_0, the expected value of their final action is

$$\langle J \rangle = \left. \frac{P_1 A_1 + P_2 A_2}{2\pi} \right|_{\lambda^*,\mu^*}, \tag{25}$$

and we have $\langle J \rangle \leq J_0$, since $P_1 + P_2 = 1$, $A_1 + A_2 = A_3 = 2\pi J_0$, and $A_i > 0$, $P_i > 0$. Therefore, the final expected action is smaller than the initial one, i.e., the Courant-Snyder invariant of the particle has been reduced. For distribution of particles with action J_0, this results in a cooling of the beam.

Furthermore, when trapping occurs at (λ^*, μ^*), we have $A_3 = 2\pi J_0$, and using $A_3 = \pi\lambda^*/2 + K_1 + K_2 = 2\pi J_0$, we obtain the expression

$$K_1 + K_2 = \pi\left(2J_0 - \frac{\lambda^*}{2}\right). \tag{26}$$

Substituting $K_1 + K_2$ into the expressions for A_1 and A_2, one obtains

$$A_1(\lambda^*, \mu^*) = \pi(\lambda^* - 2J_0) \qquad A_2(\lambda^*, \mu^*) = \pi(4J_0 - \lambda^*). \tag{27}$$

We note that the values of A_1 and A_2 at the crossing time do not depend on μ^*.

We can then rewrite $\langle J \rangle$ using $P_2 = 1 - P_1$, which gives

$$\langle J \rangle = 2J_0 - \frac{\lambda^*}{2} + P_1(\lambda^* - 3J_0) \tag{28}$$

having calculated P_1 at $\lambda = \lambda^*$, $\mu = \mu^*$.

B. Cooling protocols

We envisage three possible protocols to achieve beam cooling since we can trap particles by varying only $\lambda(t)$, only $\mu(t)$, or both parameters. We recall that, as indicated by Eq. (12), λ is proportional to the frequency of the ac-modulated magnet, while μ is proportional to its strength. We will present the three possible processes in this order, referring to them as Protocol A, B, and C, respectively.

1. Variation of λ (Protocol A)

If we keep μ constant, $\mathrm{d}A_i/\mathrm{d}t = \partial A_i/\partial\lambda \cdot \mathrm{d}\lambda/\mathrm{d}t$, and the probabilities are thus given by

$$\xi_i = \left. \frac{\mathrm{d}A_i/\mathrm{d}\lambda}{\mathrm{d}A_3/\mathrm{d}\lambda} \right|_{\lambda=\lambda^*} \qquad i = 1, 2. \tag{29}$$

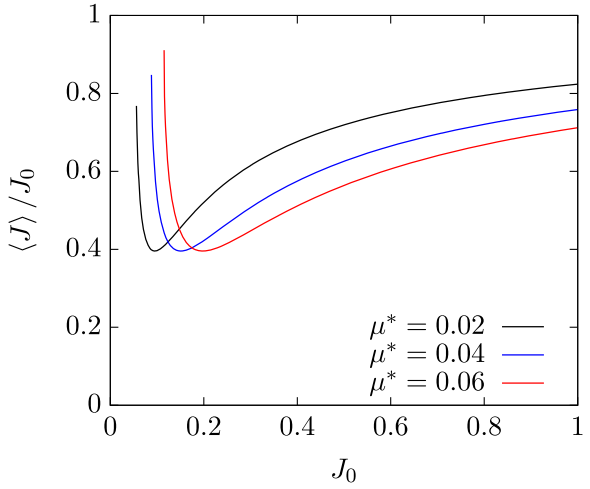

FIG. 2. Cooling ratio $\langle J \rangle / J_0$ for trapping in G_1 and G_2, with the variation of λ according to Eq. (28), for three values of μ^*.

Their expressions have been computed in [35,36] and read

$$\frac{\partial A_1}{\partial\lambda} = \frac{\Theta}{2}, \qquad \frac{\partial A_2}{\partial\lambda} = \pi - \Theta,$$
$$P_1 = \frac{\Theta/2}{\pi - \Theta/2}, \qquad P_2 = \frac{\pi - \Theta}{\pi - \Theta/2}, \tag{30}$$

where

$$\Theta = \mathrm{acos}\left(\frac{\lambda}{2x_c^2} - 2\right). \tag{31}$$

Figure 2 shows $\langle J \rangle / J_0$ as a function of J_0 for different values of μ^*. We find that the minimum value of $\langle J \rangle / J_0$ is independent of μ^* (the proof is given in the appendix).

A numerical calculation of this minimum value gives $\langle J \rangle / J_0 = 0.3957$. Given J_0, we can always find a value μ that optimizes the cooling, with the final action reduced to ≈40% of the initial value.

Generally speaking, when $\varepsilon \neq 0$, as in the final state of this protocol, the emittance is not equal to the average value of the adiabatic invariant. The reason for this is that the emittance is computed assuming that the dynamics induces a rotation around the origin, whereas the adiabatic invariant is computed with respect to the fixed point around which the initial conditions actually evolve. In fact, when $\varepsilon \neq 0$, and especially when the particles are trapped in both G_1 and G_2, as in the final state of this protocol, they do not rotate around the origin. We also observe that if such a cooled beam were transferred to another accelerator, then its emittance would indeed be equal to the average action of the particle distribution. In this sense, the cooling ratio $\langle J \rangle / J_0$ calculated from Eq. (28) is the lower bound to the actual ratio between the final and initial emittance values.

This situation could be solved or at least mitigated if it were possible to develop a protocol of adiabatic transport

that, after the trapping phase, would preserve the actions of the particles while reducing μ to zero. However, it should be considered that when trapping is achieved by means of a variation of λ only, cooling is not particularly efficient since, at best, the cooling ratio is ≈60%. The methods we will present in the following sections are, in theory, capable of achieving total cooling.

2. Variation of μ and complete trapping in G_2 (Protocol B)

For the protocol based on the variation of μ, the area derivatives ($i = 1, 2$) are given by

$$\frac{\mathrm{d}A_i}{\mathrm{d}\mu} = \frac{\mathrm{d}\alpha}{\mathrm{d}\mu}\frac{\mathrm{d}x_\mathrm{c}}{\mathrm{d}\alpha}\frac{\mathrm{d}A_i}{\mathrm{d}x_\mathrm{c}}, \tag{32}$$

where

$$\frac{\mathrm{d}\alpha}{\mathrm{d}\mu} = \frac{1}{2}\sqrt{\frac{12}{8\lambda^3 - 27\mu^2}}, \qquad \frac{\mathrm{d}x_\mathrm{c}}{\mathrm{d}\alpha} = -\frac{\sqrt{6\lambda}}{3}\sin\left(\frac{\pi}{6}+\alpha\right),$$
$$\frac{\mathrm{d}A_1}{\mathrm{d}x_\mathrm{c}} = -2\frac{(6x_\mathrm{c}^2-\lambda)^{3/2}}{x_\mathrm{c}\sqrt{2x_\mathrm{c}^2-\lambda}}, \qquad \frac{\mathrm{d}A_2}{\mathrm{d}x_\mathrm{c}} = 4\frac{(6x_\mathrm{c}^2-\lambda)^{3/2}}{x_\mathrm{c}\sqrt{2x_\mathrm{c}^2-\lambda}}. \tag{33}$$

Thus, we have $\xi_1 = -1$ and $\xi_2 = 2$, which means that $P_1 = 0$ and $P_2 = 1$. Therefore, all particles are trapped in G_2, with an action value

$$J = \frac{A_2}{2\pi} = 2J_0 - \frac{\lambda^*}{2} \tag{34}$$

Cooling is possible in the interval $\lambda^*/4 \le J_0 \le \lambda^*/2$, i.e. $2J_0 \le \lambda^* \le 4J_0$, which corresponds to the existence of square roots $\sqrt{\lambda^* - 2x_\mathrm{c}^2}$ and $\sqrt{6x_\mathrm{c}^2 - \lambda^*}$.

On the other hand, for $\lambda^* > 4J_0$, the initial condition does not belong to the outer region but to the inner region, G_1. In that case, the separatrix crossing occurs when $A_1 = 2\pi J_0$ and the particle is trapped in G_2 at an action $A_2(\lambda^*, \mu^*)/(2\pi)$. Using the expressions for A_1 and A_2, we find that the expected final action is

$$J = \frac{\lambda^*}{2} - 2J_0, \tag{35}$$

which means that cooling is also possible for $4J_0 \le \lambda^* \le 6J_0$, i.e. $\lambda^*/6 \le J_0 \le \lambda^*/2$.

After being trapped in G_2, the particle distribution has a smaller action than the initial one, but, as before, the definition of adiabatic invariant, which being $\mu \neq 0$, is not related to $(x^2 + p_x^2)/2$. Therefore, a transport process must be designed to reduce μ to zero without losing particles from G_2. Since the particles are trapped in the region G_2, we need to keep its area constant, i.e., $\mathrm{d}A_2/\mathrm{d}t = 0$, or

$$\frac{\mathrm{d}A_2}{\mathrm{d}t} = \frac{\mathrm{d}\lambda}{\mathrm{d}t}\left(\frac{\partial A_2}{\partial\lambda} + \frac{\mathrm{d}x_\mathrm{c}}{\mathrm{d}\lambda}\frac{\partial A_2}{\partial x_\mathrm{c}}\right) = 0. \tag{36}$$

This can be used to derive a differential equation for $\mu(\lambda)$

$$\frac{\mathrm{d}\mu}{\mathrm{d}\lambda} = -2x_\mathrm{c}\sqrt{\frac{\lambda - 2x_\mathrm{c}^2}{6x_\mathrm{c}^2 - \lambda}}\,\mathrm{asin}\frac{\sqrt{\lambda - 2x_\mathrm{c}^2}}{2x_\mathrm{c}}. \tag{37}$$

Following this equation, as λ is reduced, μ increases, and while A_2 remains constant, A_1 is reduced to zero, which occurs when $\mu = (2\lambda/3)^{3/2}$. We can then safely reduce both μ and λ to zero, stopping the perturbation: In fact, as μ is kept below $(2\lambda/3)^{3/2}$, no island is present in the phase space.

3. Coupled variation of λ and μ and complete trapping in G_1 (Protocol C)

One could also devise a protocol in which both λ and μ are changed. We can express μ as a function of λ, and the expression of the capture probabilities becomes

$$P_i = \left.\frac{\partial A_i/\partial\lambda + \mu'\,\partial A_i/\partial\mu}{\partial A_3/\partial\lambda + \mu'\,\partial A_3/\partial\mu}\right|_{\lambda=\lambda^*,\mu=\mu^*} \qquad i = 1, 2, \tag{38}$$

where the prime symbol denotes the derivative w.r.t. λ.

The trapping probability is calculated at the jumping point (λ^*, μ^*). Therefore, we can define an implicit function $\lambda^*(\mu)$ that resolves the equation $A_3 = A_0$ (see Fig. 3, left). Then, we optimize the probability by imposing that (i) all particles are trapped in region G_1; (ii) the area A_1 is minimized at the trapping point. For the first condition, equation $P_1 = 1$, $P_2 = 0$, gives the following condition on μ'

$$\mu' = -\left.\frac{\partial A_2/\partial\lambda}{\partial A_2/\partial\mu}\right|_{\lambda^*,\mu^*}. \tag{39}$$

Note that the signs of the partial derivatives of A_2 w.r.t. λ and μ ensure that $\mu' < 0$.

When $P_1 = 1$, $P_2 = 0$, and $2\pi\langle J\rangle = A_1 = \lambda^* - 2J_0$, we can minimize $\langle J\rangle$ by choosing the minimum λ^* for which trapping is possible. This corresponds to $A_1 = 0$, from which $\lambda^* = 2J_0$, and the equation $A_3 = 2\pi J_0$ becomes

$$K_1 + K_2 = \pi J_0, \tag{40}$$

which can be solved by setting $K_1 = \pi J_0$ and $K_2 = 0$. From $K_1 = \pi J_0$, we have the equation

$$\mathrm{asin}\left(\frac{\sqrt{2J_0 - 2x_\mathrm{c}^2}}{2x_\mathrm{c}}\right) = \frac{\pi}{2}, \tag{41}$$

which is solved when the argument of the arc-sine is 1, so

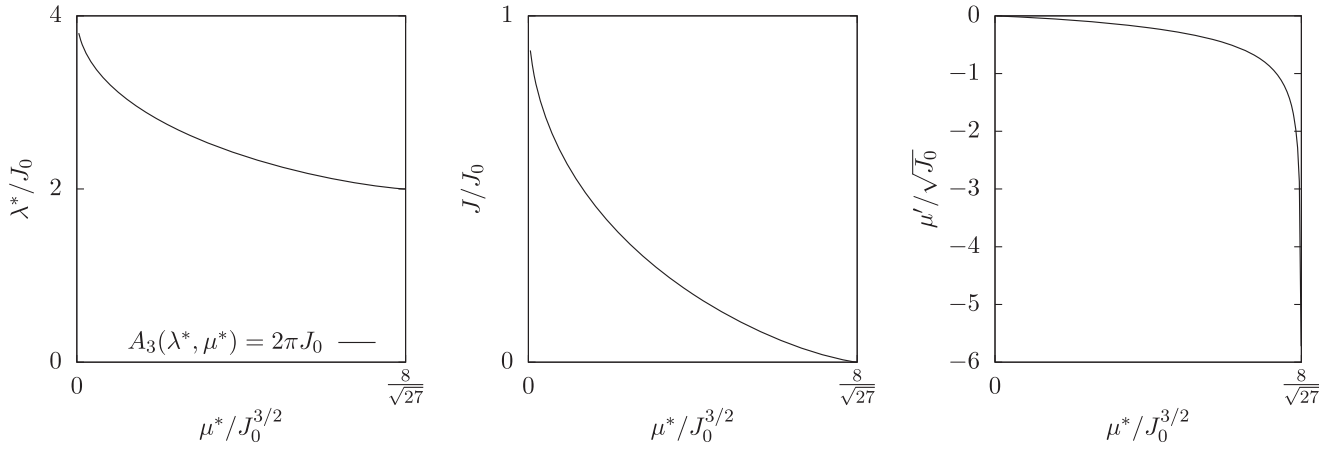

FIG. 3. Left: implicit solution $\lambda^*(\mu^*)$ of the equation $A_3(\lambda^*,\mu^*) = 2\pi J_0$. Center: expected cooling ratio J/J_0 for trapping particles via the coupled variation of λ and μ, as a function of μ^*. Right: the required value of μ' to achieve the cooling efficiency shown in the center plot, as a function of μ^*. Thanks to the ratios of variables reported on the axes, the plotted functions are unique and independent from the value of J_0.

$$\sqrt{2J_0 - 2x_c^2} = 2x_c \Rightarrow 6x_c^2 - 2J_0 = 6x_c^2 - \lambda = 0. \quad (42)$$

It is straightforward to verify that this implies $K_2 = 0$. Furthermore, this condition induces $\partial A_2/\partial\mu = 0$, and μ' to diverge. Thus, a perfect cooling, i.e., in which the final value of the action is zero, would require one to change μ infinitely fast, which contradicts the adiabatic condition we have made to apply the theoretical results.

Although it is not possible to provide an analytical expression for the implicit solution $\lambda^*(\mu^*)$ of equation $A_3 = 2\pi J_0$, we can prove that the graphs shown in Fig. 3 represent the unique solution after having properly scaled the axes. In particular, we find (the details are reported in the appendix) that the graph of the implicit solution of the equation $A_3 = 2\pi J_0$ is independent of J_0 if we rescale $\lambda^* \to \lambda^*/J_0$ and $\mu^* \to \mu^*/J_0^{3/2}$ (see Fig. 3, left). Similar laws hold for the expected cooling J/J_0, which is a function of the only variable $\mu^*/J_0^{3/2}$ (see Fig. 3, center), and for the required μ', which fulfills the functional relation $\mu'/\sqrt{J_0} = f(\mu^*/J_0^{3/2})$; see Fig. 3, right.

IV. SIMULATION RESULTS

We perform numerical simulations of the dynamics generated by the Hamiltonian of Eq. (4) varying λ and μ according to the protocols previously described. In these simulations, we set $\omega_0/(2\pi) = 0.414$, $k_3 = 1$ and invert the relations of Eq. (12) to obtain the values of ω and ε as functions of λ and μ at each time step. It is worth mentioning that although Eq. (7) provides the estimate of Ω_2, to increase precision, including higher-order contributions to the detuning generated by the dynamics of the system (4), Ω_2 has been numerically evaluated by fitting the tracking data of the system (4) at $\varepsilon = 0$. A frequency analysis of the orbits has been performed using the techniques described in [38]. With the chosen values of ω_0 and k_3, we obtained $\Omega_2 = -0.3196$, to be compared with $\Omega_2 = -0.3204$ provided by Eq. (7). The simulation times are reported in the caption of each plot and are expressed in units of turns of the accelerator represented by the Hamiltonian model. It should be stressed that, in general, the best performance in terms of emittance cooling is achieved for a total number of turns corresponding to approximately 10^5.

The initial distribution used in the simulations is an infinitely thin annular distribution with initial action $J_0 = (x_0^2 + p_{x,0}^2)/2$ while uniformly distributed according to the angle variable $\phi_0 = \mathrm{atan}(p_{x,0}/x_0)$, i.e., with pdf.

$$\rho_{J_0}(\phi, J) = \frac{\delta(J - J_0)}{2\pi}. \quad (43)$$

The distribution of Eq. (43) is not a description of a kicked beam, but its study is very useful, as the results in terms of cooling obtained with $\rho_{J_0}(\phi, J)$ can be integrated over any other distribution to obtain the corresponding cooling ratio. Furthermore, we also performed some numerical simulations using the distribution introduced in [3], which describes a Gaussian beam of zero average and standard deviation σ in x and p_x that is displaced at a distance ζ on the x axis and undergoes filamentation. Given

$$\rho^{\mathrm{a}}_{\zeta,\sigma}(x) = \mathcal{N}\ \exp\left(-\frac{x^2 + \zeta^2/2}{2\sigma^2}\right)\left[I_0\left(\frac{\zeta^2}{4\sigma^2}\right)I_0\left(\frac{\zeta x}{\sigma^2}\right) + 2\sum_{k>0}(-1)^k I_k\left(\frac{\zeta^2}{4\sigma^2}\right)I_{2k}\left(\frac{\zeta x}{\sigma^2}\right)\right], \quad (44)$$

where $\mathcal{N}$ is a normalization constant and I_k is modified Bessel function of order k (we compute the sum up to $k = 6$), we define

$$\rho^{a}_{\zeta,\sigma}(\phi, J) = \frac{1}{2\pi}\rho^{a}_{\zeta,\sigma}(x = \sqrt{2J}). \tag{45}$$

A. Protocol A: Cooling by varying λ

This protocol is divided into two phases. The first is a matching phase, to slowly adapt the initial distribution to the phase space topology, as when $\mu \neq 0$ the elliptic fixed point is shifted. We will increase μ until the chosen value μ^* while keeping $\lambda = 0$.

In the first phase, for time $t \in [0, t_1]$, we set

$$\begin{cases} \lambda(t) = 0 \\ \mu(t) = \mu^* \frac{t}{t_1}. \end{cases} \tag{46}$$

The actual trapping occurs in the second phase. The parameter λ increases linearly from 0 to a value $\Delta\lambda$. To trap particles at J_0, one needs $\Delta\lambda > \lambda^*$, where $\lambda^* = \lambda^*(\mu^*, J_0)$. We then set, for time $t \in [t_1, 2t_1]$

$$\begin{cases} \lambda(t) = \Delta\lambda\left(\frac{t-t_1}{t_1}\right) \\ \mu(t) = \mu^*. \end{cases} \tag{47}$$

We remark that although the proposed protocol, for the sake of simplicity, envisages two phases of the same duration, it is certainly possible to remove this constraint to adapt the duration of each phase to make it as adiabatic as possible.

Figure 4 shows the simulated $\langle J\rangle/J_0$ for different annular distributions ρ_{J_0} as a function of the initial action

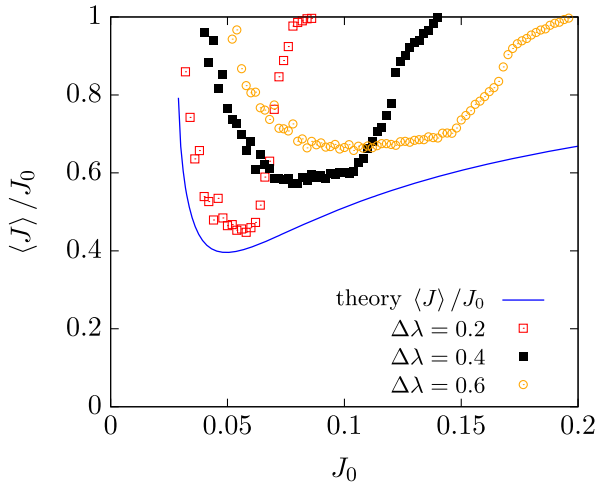

FIG. 4. Simulated cooling ratio obtained by applying Protocol A for different values of $\Delta\lambda$, as a function of the initial annular distribution action J_0. A comparison with the theoretical bound on the cooling efficiency given by Eq. (28) is presented. The Hamiltonian (4) has been used, with $k_3 = 1$, $\omega_0/(2\pi) = 0.414$, $\Omega_2 = -0.3196$, $\mu^* = 7.5 \times 10^{-3}$, $t_1 = 5 \times 10^4$.

J_0 using three values of $\Delta\lambda$ (with $\mu^* = 7.5 \times 10^{-3}$) and compares it with the theoretical estimate given by Eq. (28). We note that the scales of λ and μ are related to that of J_0 and therefore the selected values of μ^* do not have any specific meaning since any change would simply rescale the J_0 axis in Fig. 4.

We observe two effects that are the root of the difference between the theoretical reduction of $\langle J\rangle/J_0$ and the observed behavior. For higher values of $\Delta\lambda$, the cooling range is increased at the expense of the minimum cooling ratio. Given $\Delta\lambda$ and μ^*, for large values of J_0, λ is never big enough to achieve trapping since the value of λ^* that solves $A_3(\lambda^*, \mu^*)$ is larger than $\Delta\lambda$. Furthermore, increasing $\Delta\lambda$ to trap more particles moves the center of G_2 far from the origin of the phase space (all fixed points of Eq. (13), from the solution of the resulting cubic equation, are $O(\sqrt{\lambda})$ for large values of λ), thus decreasing the effective cooling ratio.

B. Protocol B: Cooling by varying μ

This protocol consists of three phases: the first phase is used to perform particle trapping, and the second and third phase is needed to transport the particles back to the center of the phase space by progressively reducing the strength of the ac dipole.

In the first phase, for times $t \in [0, t_1]$, we have the following:

$$\begin{cases} \lambda(t) = \lambda^* \\ \mu(t) = \mu_1 \frac{t}{t_1}, \end{cases} \tag{48}$$

and the condition $\mu_1 > \mu^*$, where μ^* solves the equation $A_3(\lambda^*, \mu^*) = 2\pi J_0$.

In the second phase, the differential equation (36) is solved. For $t \in [t_1, t_2]$, we set $\lambda(t) = \lambda^* - \dot{\lambda}(t - t_1)$ and obtain $\mu(t)$ by numerically integrating the Cauchy problem

$$\begin{cases} \frac{d\mu}{dt} = \frac{d\lambda}{dt}\frac{d\mu}{d\lambda} = -\dot{\lambda}\frac{d\mu}{d\lambda} \\ \mu(t_1) = \mu_1, \end{cases} \tag{49}$$

where $d\mu/d\lambda$ is given by Eq. (36). The second phase is stopped at time t_2 once condition $\mu(t_2) = \mu_2 = (2\lambda(t_2)/3)^{3/2}$ is met. The third phase follows for times $t \in [t_2, t_3]$ ($t_3 = t_1 + t_2$), with

$$\begin{cases} \lambda(t) = \lambda(t_2)\left[1 - \left(\frac{t-t_2}{t_1}\right)\right] \\ \mu(t) = \left(\frac{2}{3}\lambda(t)\right)^{3/2} \end{cases}. \tag{50}$$

The plots of the time evolution of λ and μ are shown in Fig. 5.

Figure 6 shows the simulated cooling ratio $\langle J\rangle/J_0$, as a function of λ^*, for an initial annular distribution $\rho_{J_0}(\phi, J)$ with $J_0 = 0.05$, together with the theoretical expected

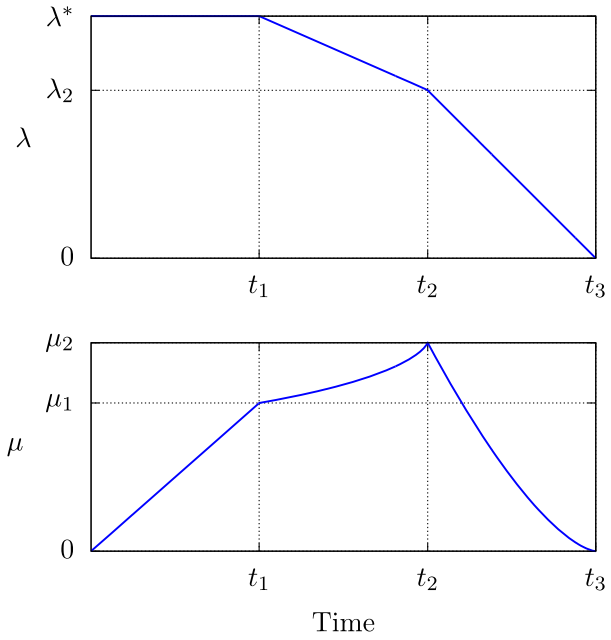

FIG. 5. Evolution of $\lambda(t)$ and $\mu(t)$ during the three phases of Protocol B.

value given by Eqs. (34) and (35). In order to introduce only one time scale in our simulations, we adapt the time step of the numerical integration of Eq. (49) so that we always have $t_2 = 2t_1$.

We note that the theory presented earlier accurately describes the simulated cooling ratio unless it is in the vicinity of $\lambda^* = 4J_0 = 0.2$, where the theory predicts total cooling, while in simulation, $\langle J\rangle/J_0 \approx 10\%$. This is due to the angular dependence on which we averaged in our analysis, as can be inferred from Fig. 7. This figure shows

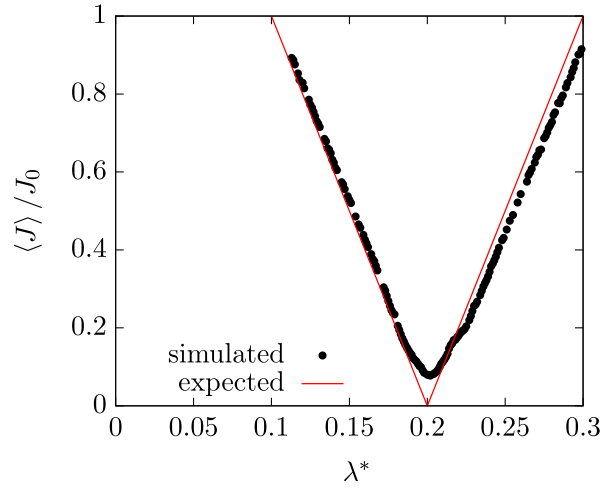

FIG. 6. Expected and simulated cooling ratio for trapping in G_2 using Protocol B as a function of λ^*. The initial distribution is $\rho_{0.05}$. The Hamiltonian (4) has been used, with $k_3 = 1$, $\omega_0/(2\pi) = 0.414$, $\Omega_2 = -0.3196$, $\mu_1 = 0.02$, $t_1 = 1/\dot{\lambda} = 5 \times 10^4$.

the distributions at the end of each of the three phases of Protocol B for the same initial annular distribution for three values of λ^*. We observe that at the end of each phase, the action of the particles, which were all the same at the beginning, spreads according to their initial phase. For example, red particles, which correspond to the initial phase π, result in the innermost position when $\lambda^* = 0.15$ and in the outermost position when $\lambda = 0.25$. This behavior reverses for cyan particles, which have $\phi_0 = 0$. This means that particles with different initial angles are trapped at slightly different values of J. Some particles are trapped earlier or later than expected, with a larger or smaller value of J than that given by theory. In the graphs, it is also visible that the inner and outer particles are reversed, depending on whether $\lambda^* < 4J_0$ or $\lambda^* > 4J_0$. However, when $\lambda \approx 4J_0$, all particles are trapped at a higher value than expected, regardless of when they cross the separatrix, thus increasing $\langle J\rangle$. In our simulations, we were able to reach $\langle J\rangle/J_0 = 0.078$, for a cooling efficiency of 92%.

In Fig. 8 (top), we show the dependence of the cooling ratio on the value of the initial action J_0 for three values of λ^*. The range in which $\langle J\rangle/J_0 < 1$ represents the possible interval of actions of a thick annular distribution that could be cooled using Protocol B. Note that according to theoretical predictions, cooling is possible in the range $\lambda^*/6 \leq J_0 \leq \lambda^*/2$ and the optimal cooling ratio is found at $J_0 = \lambda^*/4$. An animation of the trapping process for a thick annular distribution is available as Supplemental Material [39].

In Fig. 8 (bottom), the cooling for the case of a distribution such as Eq. (45) is shown as a function of σ_0 of the Gaussian function before filamentation. Note that the parameter ζ is the same for the three cases of λ^* considered. The curves have a similar structure: they have an initial plateau of increasing length for a decreasing value of λ^* and then a rather linear increase for increasing values of σ_0. The difference between the three curves is mainly determined by the value of ζ and the position of the minimum cooling visible in Fig. 8 (top).

C. Protocol C: Cooling by varying λ and μ

This protocol requires two phases: the first to adapt the phase space and the second for trapping and transport. Our goal, in addition to trapping the particles inside G_1, is to ensure that both at the beginning and at the end of the process, the adiabatic invariant is as close as possible to the linear action variable $J = (x^2 + p_x^2)/2$, which is true if the ac dipole is turned off, i.e., when $\mu = 0$. Thus, in the first phase, μ gradually increases, while keeping $\lambda = 0$ (i.e., $\omega = \omega_0$), until it reaches the value needed to initiate the trapping process. In the second phase, the derivative of $\mu(\lambda)$ remains at a constant value μ', while increasing λ and taking advantage of the fact that as $\mu' < 0$, we can slowly reduce μ until it reaches zero to recover the equivalence between the adiabatic invariant and J.

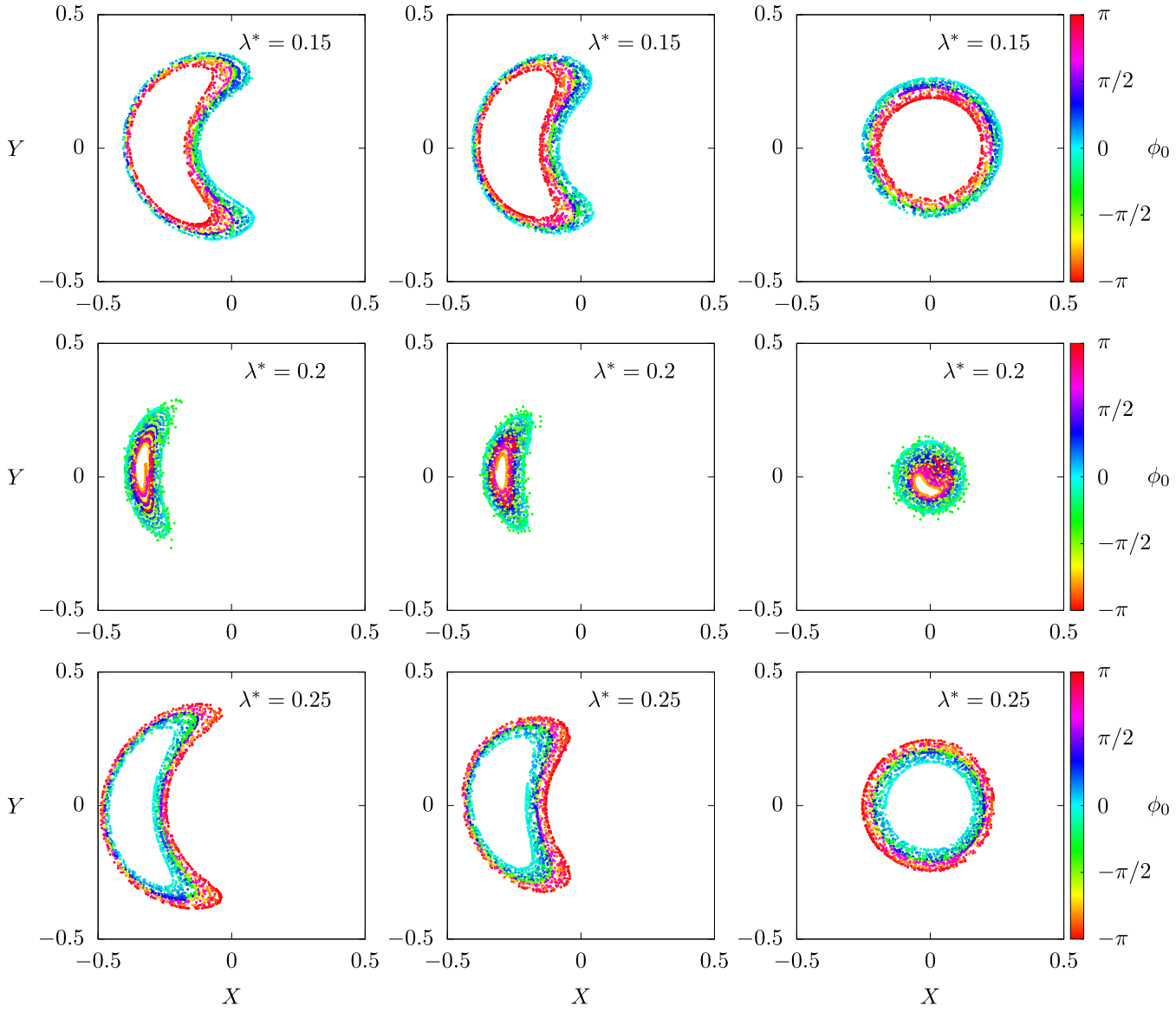

FIG. 7. Distributions at the end of the first (left), second (center), and third (right) phase for an initial distribution $\rho_{0.05}$ for Protocol B for three values of λ^*. The color scale represents the initial angle ϕ_0 and the initial distribution is the same as that shown in the left plots of Fig. 11. Note that for $\lambda^* > 4J_0 = 0.2$, the angular dependence of the final action is reversed w.r.t. $\lambda^* < 0.2$. The Hamiltonian of Eq. (4) has been used, with $k_3 = 1$, $\omega_0/(2\pi) = 0.414$, $\Omega_2 = -0.3196$, $\mu_1 = 0.02$, and $t_1 = 1/\dot{\lambda} = 5 \times 10^4$.

In the first phase, for times $t \in [0, t_1]$, we set

$$\begin{cases} \lambda(t) = 0 \\ \mu(t) = \mu_{\max} \frac{t}{t_1}, \end{cases} \tag{51}$$

where $\mu_{\max} = \mu^* + \lambda^* |\mu'|$. This ensures that during the second phase when $\lambda = \lambda^*$, μ is exactly μ^* and its derivative μ' has the appropriate value. The values of μ^* and λ^* are obtained by choosing a solution of the implicit equation $A_3 = A_0$ for the selected value of J_0 that corresponds to the desired cooling. From Eq. (39), the desired value of μ' is also calculated.

In the second phase, where $t \in [t_1, 2t_1]$, we have

$$\begin{cases} \lambda(t) = \frac{\mu_{\max}}{|\mu'|} \left(\frac{t - t_1}{t_1} \right) \\ \mu(t) = \mu_{\max} - |\mu'| \lambda(t). \end{cases} \tag{52}$$

When the process ends and $\mu = 0$ is reached, G_2 disappears, as the perturbation provided by the ac dipole has been turned off and the particles trapped in G_1 have been transported to the center of the phase space. The values of λ and μ during the whole procedure are plotted in Fig. 9.

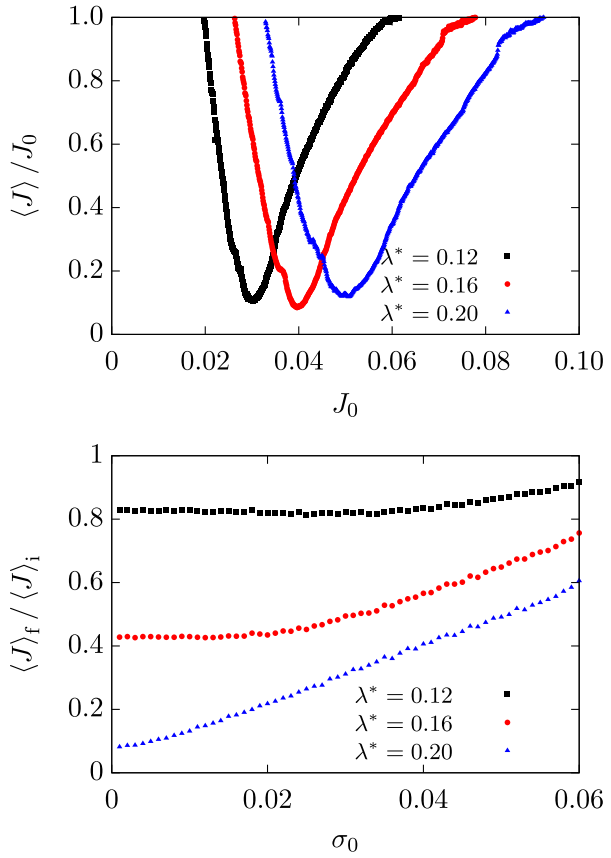

FIG. 8. Top: cooling ratio for trapping in G_2 using Protocol B, at different values of λ^*, as a function of the initial action of the annular distribution J_0. Bottom: cooling ratio for the same values of λ^* as a function of σ_0, using the initial distribution $\rho^{a}_{\zeta,\sigma_0}(J_0,\phi)$ defined in Eq. (45) with $\zeta = 0.05$. $\langle J\rangle_i$ is the average of the initial actions. The Hamiltonian (4) has been used, with $k_3 = 1$, $\omega_0/(2\pi) = 0.414$, $\Omega_2 = -0.3196$, $\mu_1 = 0.02$, and $t_1 = 1/\dot{\lambda} = 5 \times 10^4$.

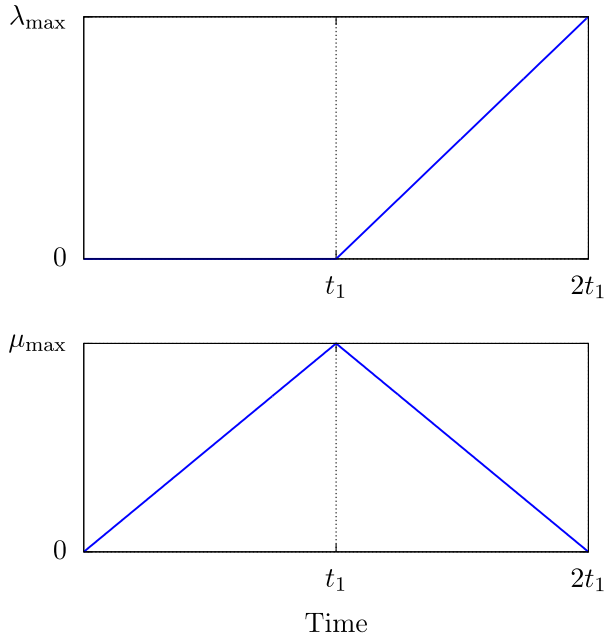

FIG. 9. Evolution of $\lambda(t)$ and $\mu(t)$ during the two phases of Protocol C. The two values λ_{max} and μ_{max} have expressions in function of the computed λ^*, μ^*, and μ', i.e., $\mu_{max} = \mu^* + \lambda|\mu'|$, $\lambda_{max} = \lambda^* + \mu^*/|\mu'|$.

We remark that although the proposed protocol envisages two phases of the same duration, it is possible to remove this constraint to adapt the duration of each phase to make them as adiabatic as possible.

In Fig. 10, we show the simulated cooling ratio $\langle J\rangle/J_0$ for an initial annular distribution $\rho_{0.05}(\phi, J)$, as a function of μ^*, and a comparison with the theoretically expected value $\langle J\rangle = (\lambda^*(\mu^*) - 2J_0)/(2\pi)$. It can be seen that the agreement between theory and simulation is notable up to a certain breakdown value of μ^*. This breakdown is due to the angular dynamics, which has been neglected in the averaging process of the theory. In Fig. 11, we show the initial distribution, the situation at the end of the first phase, and the final distribution of particles for two different values of μ^*, using the hue to represent the initial angle ϕ_0. For both values of μ^*, we observe that the distribution after the first phase is no longer infinitely thin and that the action of each particle depends on the initial angle. As a result, each particle crosses the separatrix at a different time at the end of the second phase, resulting in different values of the final action. For μ^* smaller than the breakdown threshold, all particles are still trapped in G_1, and this angular dependence is averaged out. On the other hand, for higher values of μ^*, particles, which are at the end of the first phase, are in the outer part of the distribution and can also be trapped in G_2 at high amplitude, thus dramatically increasing the value of the final action. We again stress that we cannot expect to reach 100% cooling, since $|\mu'|$ and μ_{max} would need to reach unlimited values. The best cooling that we could achieve in our numerical simulations is 92%, at $\langle J\rangle/J_0 = 0.08$.

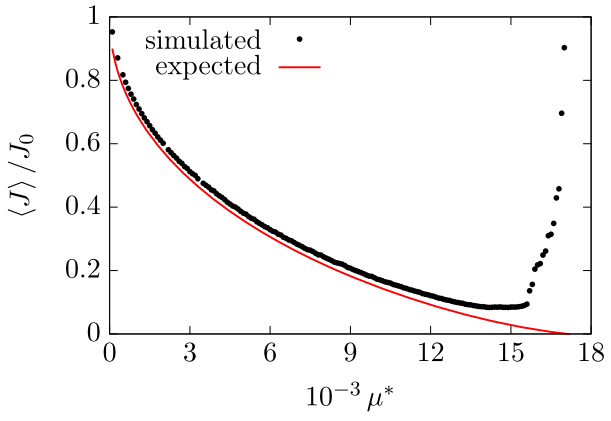

FIG. 10. Expected and simulated cooling ratio for trapping in G_1 using Protocol C as a function of μ^* for an initial distribution $\rho_{0.05}$. The Hamiltonian (4) has been used, with $k_3 = 1$, $\omega_0/(2\pi) = 0.414$, $\Omega_2 = -0.3196$, and $t_1 = 1 \times 10^5$.

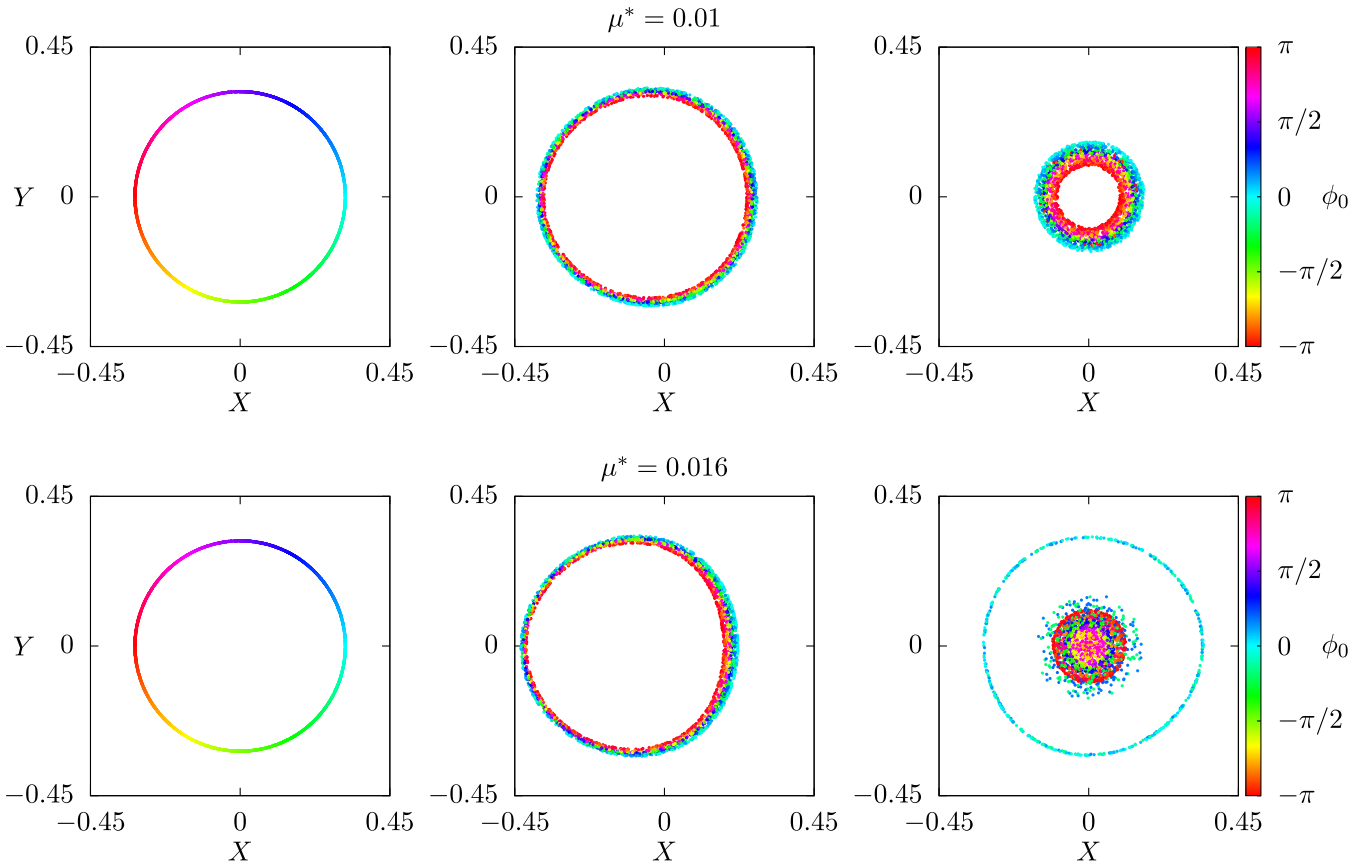

FIG. 11. Particle distributions when applying Protocol C at the beginning (left), after the first phase (middle), and at the end of the second phase (right), for two values of μ^*. The hue encodes the initial angle of the action distribution. The Hamiltonian (4) has been used, with $k_3 = 1$, $\omega_0/(2\pi) = 0.414$, $\Omega_2 = -0.3196$, $t_1 = 1 \times 10^5$.

To study the applicability of the cooling protocol to a more realistic particle distribution, we have looked at an ensemble of infinitely thin annular distributions ρ_{J_0} covering a certain interval in J_0. The values of μ' and $\mu_{\max}$ have been chosen to optimize the trapping for a particular value of J_0, $\hat{J}_0 = 0.05$. The results are shown in Fig. 12 (top). It is clearly visible that for different values of μ^*, which translate into different cooling targets for particles at $\hat{J}_0$, a significant range of action values is actually cooled. The width of this *cooling well*, i.e., the range of J_0, where $\langle J \rangle / J_0 < 1$, is the thickness of the annular distribution that the protocol can handle successfully. We note that, contrary to theoretical expectations, the minimum value of $\langle J \rangle / J_0$ does not occur at $\hat{J}_0$, although this difference tends to decrease as μ^* increases.

In Fig. 12 (bottom), the cooling for the case of a distribution such as Eq. (45) is shown as a function of σ_0 of the Gaussian function before filamentation. Note that the parameter ζ is the same for the three cases of μ^* considered. The curves have a similar structure: they feature an initial plateau of increasing length for decreasing values of μ^* and then an increase for increasing values of σ_0 that is not linear. The difference between the three curves is smaller than for the case shown in Fig. 8 (bottom) because the position of the minimum cooling visible in Fig. 12 (top) does not change much.

This is again due to angular dynamics. Using the same parameters as the plots shown in Fig. 12, two final distributions are shown in Fig. 13 using the color hue to identify the initial phase. The right graph shows the case where the initial distribution is $\rho_{0.05}$, i.e., the initial conditions are selected at $\hat{J}_0$, while the left graph shows the case where the initial distribution is $\rho_{0.045}$, where the initial actions have a value $J_0 < \hat{J}_0$, but close to the minimum. In the left plot, a gap in the final distribution is clearly visible. This can be explained by the fact that, in this case, some particles are trapped earlier (the red dots in the plots) because of the spread of the action after the first phase. These can end up in G_2 or in G_1, according to the probability law, but when their areas are smaller. Therefore, the average final action is reduced more by this effect than by the increase induced by the particles in G_2.

An animation of the trapping process for a thick annular distribution is available as Supplemental Material [39].

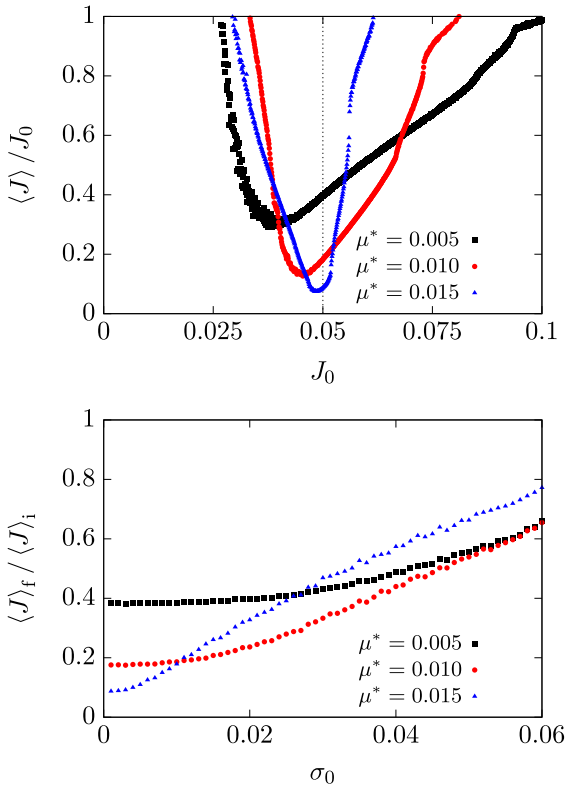

FIG. 12. Top: simulated cooling ratio $\langle J\rangle/J_0$ for initial distributions ρ_{J_0} using Protocol C at different values of μ^*, having computed μ' and $\mu_{\max}$ for $J_0 = \hat{J}_0 = 0.05$ (indicated by a vertical dotted line in the plot). Bottom: cooling ratio for the same values of μ^* as a function of σ_0, using the initial distribution $\rho^{a}_{\zeta,\sigma_0}(J_0,\phi)$ defined in Eq. (45) with $\zeta = 0.05$. $\langle J\rangle_i$ is the average of the initial actions. The Hamiltonian (4) has been used, with $k_3 = 1$, $\omega_0/(2\pi) = 0.414$, $\Omega_2 = -0.3196$, and $t_1 = 1\times 10^5$.

V. CONCLUSIONS

In this paper, beam manipulations based on nonlinear beam dynamics have been devised with the goal of achieving cooling for annular transverse beam distributions. Such a beam distribution can be generated after a beam is kicked in the transverse direction. The possibility of achieving cooling by means of crossing stable resonances generated by static magnetic elements has been ruled out; however, the use of an ac dipole for such manipulations has proven to be very successful.

A Hamiltonian model describing the transverse dynamics in the presence of an ac dipole has been studied using concepts from adiabatic theory for Hamiltonian systems. This has allowed the design of three cooling protocols, two of which have proven to be extremely effective with a simulated best cooling performance of ≈90%, which is achieved over a timescale of approximately 10^5 turns of the accelerator represented by the Hamiltonian model considered in our studies. In physical terms, the observed cooling is achieved by controlling the strength and frequency of the ac dipole according to the specifications of the proposed protocols.

The Hamiltonian model used for our studies includes amplitude detuning from single-particle nonlinear effects in the 4D transverse phase space, and the final analysis can be carried out in 2D. Low-order resonances excited by nonlinear effects, which might spoil the phase space topology that is generated by the ac dipole used for the beam cooling protocols presented in this paper, are not included in the model studied. This does not seem to be a serious limitation, as, in general, circular accelerators are operated far from this type of resonance. Higher-order resonances

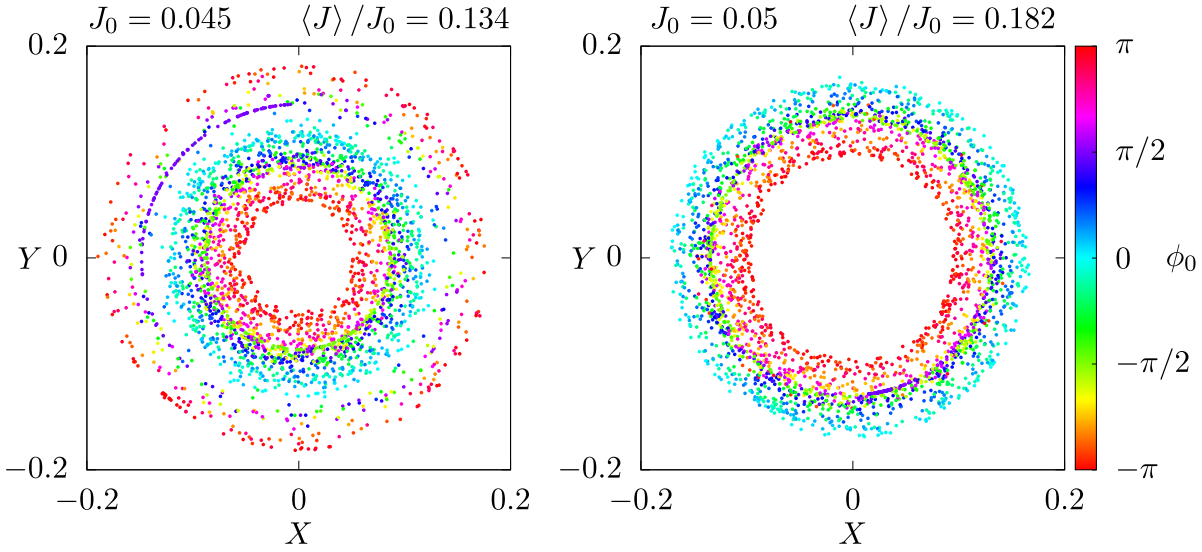

FIG. 13. Final particle distributions after applying Protocol C, for initial distributions $\rho_{0.045}$ (left) and $\rho_{0.05}$ (right), having computed μ' for $\hat{J}_0 = 0.05$. The hue indicates the initial angle ϕ_0. We see that, although the process has been optimized for $\hat{J}_0 = 0.05$, for $J_0 < \hat{J}_0$ (and close to the minimum shown in Fig. 12), the resulting cooling is better. The Hamiltonian (4) has been used, with $k_3 = 1$, $\omega_0/(2\pi) = 0.414$, $\Omega_2 = -0.3196$, $t_1 = 1\times 10^5$, and $\mu^* = 0.01$.

have a much smaller effect on trapping and transport phenomena, which is why they have not been included in our analysis. The coupling of synchrotron motion with transverse betatron dynamics has also been neglected. This coupling manifests itself, in the presence of finite chromaticity, as a modulation of the transverse tunes. Potentially, this has an adverse impact on the trapping and transport phenomena that are at the heart of the method presented in this paper. However, reducing the chromaticity value is an efficient mitigation measure, as has been experimentally observed on the CERN MTE.

Detailed numerical simulations carried out on the considered Hamiltonian systems have revealed a rich phenomenology that could be explained in detail by using adiabatic theory for Hamiltonian systems. Although an infinitely thin annular distribution was initially used, the two best protocols have been shown to have a significant cooling range. It, therefore, seems possible to use them to cool a transverse annular beam distribution of finite thickness. Numerical studies of realistic distributions representing a filamented Gaussian have been carried out, which confirm the possibility of achieving cooling even for these distributions. These results are important in view of experimental tests at the CERN Proton Synchrotron.

Such annular beam distributions can also be representative of the beam halo, which opens up the study of future applications to halo manipulation that could result in experimental tests at the LHC. The critical aspect to be examined and evaluated in future theoretical studies is to ensure that beam halo manipulation does not damage the main beam, especially in terms of emittance.

ACKNOWLEDGMENTS

We would like to express our warm thanks to Dr. X. Buffat for motivating discussions on the topic of this paper.

APPENDIX: SOME PROOFS

Some interesting and useful properties of the theoretical laws that describe the parameters of the cooling protocols described in this paper can be derived by reasoning on the functional dependencies. Note that in the following, $f(x)$, $g(x)$, $A(x)$, $B(x)$, etc. represent generic functions of the only variable x, and the same happens for their product, i.e., $f(x)g(x) = h(x)$.

1. Uniqueness of the minimum of $\langle J\rangle/J_0$ for Protocol A

From the expressions of x_c, K_1, K_2, and Θ [see Eqs. (14), (15), (21), (22), and (31)], we define $\chi = \mu/\lambda^{3/2}$, and we can express these quantities as $x_c = \sqrt{\lambda}\tilde{x}_c(\chi)$, $K_i = \lambda\tilde{K}_i(\chi)$, and $\Theta = \Theta(\chi)$.

From the relation $A_3 = 2\pi J_0$, we have $J_0 = \lambda^* f(\chi^*)$, while from Eq. (28), we find $\langle J\rangle = \lambda^* g(\chi^*)$. Therefore, setting $h(\chi) = g(\chi)/f(\chi)$, we finally have $\langle J\rangle/J_0 = h(\chi^*)$. From the expression of $f(\chi^*) = \langle J\rangle/\lambda^*$, noting that $g(\chi^*) = J_0/\lambda^*$ is monotone (see Fig. 3, left), it is possible to show that the function $h(\chi^*)$ has a minimum for a value $\hat{\chi}^*$.

Then, there exists only one pair (λ^*, μ^*) that solves $A_3 = 2\pi J_0$ and for which $\mu^*/\lambda^{*3/2} = \hat{\chi}^*$. Therefore, for each J_0, there exists only one value $\hat{\chi}^*$ and, therefore, a unique value of $h(\hat{\chi}^*)$, which does not depend on μ^*. This proves what has been observed in Sec. III B 1.

2. Scaling laws for Protocol C

A similar approach can be used to derive the scaling laws of Sec. III B 3. As $A_3 = \lambda^*\tilde{A}_3(\chi^*)$, the equation defining the invariant after trapping reads

$$\lambda^*\tilde{A}_3(\chi^*) = \lambda^*\tilde{A}_3\left(\frac{\mu^*}{\lambda^{*3/2}}\right) = 2\pi J_0. \tag{A1}$$

The functional equation

$$xf\left(\frac{y}{x^\alpha}\right) = 2\pi z \tag{A2}$$

under the transformations $\bar{x} = x/z$, $\bar{y} = y/z^\alpha$ becomes

$$\bar{x}f\left(\frac{\bar{y}}{\bar{x}^\alpha}\right) = 2\pi, \tag{A3}$$

and this implicit equation is solved by the function $\bar{x} = g(\bar{y})$, from which we infer that, after rescaling $\lambda^* \to \lambda^*/J_0$ and $\mu^* \to \mu^*/J_0^{3/2}$, the function

$$\frac{\lambda^*}{J_0} = A\left(\frac{\mu^*}{J_0^{3/2}}\right) \tag{A4}$$

represents the unique solution to Eq. (A1). This explains the scaling shown in Fig. 3 (left).

Moreover, inverting Eq. (A1), one finds that χ^* can be written as a function of λ^*/J_0 and therefore of $\mu^*/J_0^{3/2}$:

$$\chi^* = \chi^*\left(\frac{\lambda^*}{J_0}\right) = \chi^*\left[A\left(\frac{\mu^*}{J_0^{3/2}}\right)\right] = \chi^*\left(\frac{\mu^*}{J_0^{3/2}}\right). \tag{A5}$$

Therefore, we can find a scaling law for the expected cooling ratio, as $2\pi J = A_1 = \lambda^*\tilde{A}_1(\chi^*)$, and using Eqs. (A4) and (A5), one obtains

$$\begin{aligned}\frac{J}{J_0} = \frac{\lambda^*}{J_0}\tilde{J}(\chi^*) &= A\left(\frac{\mu^*}{J_0^{3/2}}\right)\tilde{J}\left[\chi\left(\frac{\mu^*}{J_0^{3/2}}\right)\right] \\ &= B\left(\frac{\mu^*}{J_0^{3/2}}\right),\end{aligned} \tag{A6}$$

which explains the scaling shown in Fig. 3 (center).

In the same way, the coefficient μ', from the expressions of $\partial A_2/\partial\lambda$ and $\partial A_2/\partial\mu$ in Eqs. (30) and (31), can be written as

$$\mu' = \sqrt{\lambda}\,\tilde{\mu}'(\chi), \tag{A7}$$

and, dividing by $\sqrt{J_0}$ and using the functional dependencies of Eqs. (A4) and (A5), one obtains

$$\frac{\mu'}{\sqrt{J_0}} = \sqrt{\frac{\lambda^*}{J_0}}\tilde{\mu}'(\chi^*) = C\left(\frac{\mu^*}{J_0^{3/2}}\right), \tag{A8}$$

which is the scaling for the plot shown in Fig. 3 (right).

[1] R. Cappi and M. Giovannozzi, Novel Method for Multiturn Extraction: Trapping Charged Particles in Islands of Phase Space, Phys. Rev. Lett. **88**, 104801 (2002).

[2] R. Cappi and M. Giovannozzi, Multiturn extraction and injection by means of adiabatic capture in stable islands of phase space, Phys. Rev. ST Accel. Beams **7**, 024001 (2004).

[3] A. Franchi, S. Gilardoni, and M. Giovannozzi, Progresses in the studies of adiabatic splitting of charged particle beams by crossing nonlinear resonances, Phys. Rev. ST Accel. Beams **12**, 014001 (2009).

[4] J. Borburgh, S. Damjanovic, S. Gilardoni, M. Giovannozzi, C. Hernalsteens, M. Hourican, A. Huschauer, K. Kahle, G. Le Godec, O. Michels, and G. Sterbini, First implementation of transversely split proton beams in the CERN Proton Synchrotron for the fixed-target physics programme, Europhys. Lett. **113**, 34001 (2016).

[5] S. Abernethy *et al.*, Operational performance of the CERN injector complex with transversely split beams, Phys. Rev. Accel. Beams **20**, 014001 (2017).

[6] A. Huschauer, A. Blas, J. Borburgh, S. Damjanovic, S. Gilardoni, M. Giovannozzi, M. Hourican, K. Kahle, G. Le Godec, O. Michels, G. Sterbini, and C. Hernalsteens, Transverse beam splitting made operational: Key features of the multiturn extraction at the CERN Proton Synchrotron, Phys. Rev. Accel. Beams **20**, 061001 (2017).

[7] S.-Y. Lee, K. Y. Ng, H. Liu, and H. C. Chao, Evolution of Beam Distribution in Crossing a Walkinshaw Resonance, Phys. Rev. Lett. **110**, 094801 (2013).

[8] A. Bazzani, F. Capoani, and M. Giovannozzi, Manipulation of transverse emittances in circular accelerators by crossing nonlinear 2D resonances, Eur. Phys. J. Plus **137**, 594 (2022).

[9] G. I. Budker, An effective method of damping particle oscillations in proton and antiproton storage rings, Sov. At. Energy **22**, 438 (1967).

[10] S. Van Der Meer, Stochastic cooling and the accumulation of antiprotons, Rev. Mod. Phys. **57**, 689 (1985).

[11] S. Schröder *et al.*, First Laser Cooling of Relativistic Ions in a Storage Ring, Phys. Rev. Lett. **64**, 2901 (1990).

[12] P. Chen and R. B. Palmer, Coherent Paier creation as a positron source for linear colliders, AIP Conf. Proc. **279**, 888 (1992).

[13] H. Okamoto, A. M. Sessler, and D. Möhl, Three-Dimensional Laser Cooling of Stored and Circulating Ion Beams by Means of a Coupling Cavity, Phys. Rev. Lett. **72**, 3977 (1994).

[14] R. B. Palmer, Accelerator parameters for $\gamma-\gamma$ colliders, Nucl. Instrum. Methods Phys. Res., Sect. A **355**, 150 (1995).

[15] J. S. Hangst, J. S. Nielsen, O. Poulsen, P. Shi, and J. P. Schiffer, Laser Cooling of a Bunched Beam in a Synchrotron Storage Ring, Phys. Rev. Lett. **74**, 4432 (1995).

[16] V. Telnov, Laser Cooling of Electron Beams for Linear Collider, Phys. Rev. Lett. **78**, 4757 (1997).

[17] Z. Huang and R. D. Ruth, Laser-Electron Storage Ring, Phys. Rev. Lett. **80**, 976 (1998).

[18] T. Ohgaki and I. Endo, Simulation of laser-compton cooling of electron beams for future linear colliders, Phys. Rev. ST Accel. Beams **4**, 111001 (2001).

[19] Y. Yuri and H. Okamoto, Feasibility of beam crystallization in a cooler storage ring, Phys. Rev. ST Accel. Beams **8**, 114201 (2005).

[20] A. Bazzani, G. Servizi, E. Todesco, and G. Turchetti, A normal form approach to the theory of nonlinear betatronic motion, CERN, Geneva, CERN Yellow Reports: Monographs, Report No. CERN-94-02, 1994, 10.5170/CERN-1994-002.

[21] M. Giovannozzi, D. Quatraro, and G. Turchetti, Generating unstable resonances for extraction schemes based on transverse splitting, Phys. Rev. ST Accel. Beams **12**, 024003 (2009).

[22] A. Bazzani, F. Capoani, and M. Giovannozzi, Analysis of adiabatic trapping phenomena for quasi-integrable area-preserving maps in the presence of time-dependent exciters, Phys. Rev. E **106**, 034204 (2022).

[23] S. Peggs and C. Tang, Nonlinear diagnostics using an AC dipole, Brookhaven National Laboratories, Report No. RHIC/AP/159, 1998.

[24] M. Bai, Beam manipulation with an RF dipole, in *Proceedings of the 18th Particle Accelerator Conference, New York, 1999* (IEEE, New York, 1999), Vol. 1, pp. 387–391.

[25] R. Tomás, Normal form of particle motion under the influence of an ac dipole, Phys. Rev. ST Accel. Beams **5**, 054001 (2002).

[26] R. Tomás, Adiabaticity of the ramping process of an ac dipole, Phys. Rev. ST Accel. Beams **8**, 024401 (2005).

[27] R. Miyamoto, S. E. Kopp, A. Jansson, and M. J. Syphers, Parametrization of the driven betatron oscillation, Phys. Rev. ST Accel. Beams **11**, 084002 (2008).

[28] S. White, E. Maclean, and R. Tomás, Direct amplitude detuning measurement with ac dipole, Phys. Rev. ST Accel. Beams **16**, 071002 (2013).

[29] N. Biancacci and R. Tomás, Using ac dipoles to localize sources of beam coupling impedance, Phys. Rev. Accel. Beams **19**, 054001 (2016).

[30] F. S. Carlier, R. Tomás, E. H. Maclean, and T. H. B. Persson, First experimental demonstration of forced dynamic aperture measurements with LHC ac dipoles, Phys. Rev. Accel. Beams **22**, 031002 (2019).

[31] M. Giovannozzi *et al.*, The CERN PS multi-turn extraction based on beam splittting in stable islands of transverse phase space: Design report, CERN, Geneva, CERN Yellow Reports: Monographs, Report No. CERN-2006-011, 2006, 10.5170/CERN-2006-011.

[32] The typical relative accuracy of an emittance measurement at the CERN Proton Synchrotron is 5%.
[33] E. D. Courant and H. S. Snyder, Theory of the alternating-gradient synchrotron, Ann. Phys. (N.Y.) **3**, 1 (1958).
[34] A. Bazzani, S. Siboni, and G. Turchetti, Diffusion in Hamiltonian systems with a small stochastic perturbation, Physica (Amsterdam) **76D**, 8 (1994).
[35] A. I. Neishtadt, A. A. Vasil'ev, and A. V. Artem'ev, Capture into resonance and escape from it in a forced nonlinear pendulum, Regul. Chaotic Dyn. **18**, 686 (2013).
[36] A. I. Neishtadt, Passage through a separatrix in a resonance problem with a slowly-varying parameter, J. Appl. Math. Mech. **39**, 594 (1975).
[37] V. I. Arnol'd, V. V. Kozlov, and A. I. Neishtadt, Mathematical aspects of classical and celestial mechanics, *Dynamical Systems III*, 3rd rev. version, Encyclopaedia of Mathematical Sciences (Springer, Heidelberg, 2006).
[38] R. Bartolini, M. Giovannozzi, W. Scandale, A. Bazzani, and E. Todesco, Precise measurement of the betatron tune, Part. Accel. **55**, 1 (1996).
[39] See Supplemental Material at http://link.aps.org/supplemental/10.1103/PhysRevAccelBeams.26.024001 for an animation showing the evolution of an initial thick annular distribution under Protocol B and Protocol C.